Polycrystalline Indium Oxide Thin-Film Transistors formed by Solid-Phase Crystallization

Mamoru Furuta, Mir Mutakabbir Alom*, Xiaoqian Wang*, Yusaku Magari**,*
*Kochi University of Technology, Kochi, Japan
**Hokkaido University, Sapporo, Japan

Abstract

We demonstrate polycrystalline indium oxide (poly-InO_x:H) thin-film transistors (TFTs) with bottom-gate (BG) and self-aligned top-gate (SATG) structures. The poly-InO_x:H channel was formed by low-temperature solid-phase crystallization of a hydrogen-doped amorphous InO_x:H film. Both BG and SATG poly-InO_x:H TFTs operated in enhancement mode with field-effect mobilities of 32.0 $cm^2V^{-1}s^{-1}$ for BG and 29.5 $cm^2V^{-1}s^{-1}$for SATG. Furthermore, the poly-InO_x:H TFTs exhibited excellent stability under a negative gate bias and temperature stress, irrespective of the TFT structure. These results demonstrate that poly-oxide is a strong candidate for opening a new route to improve the mobility and reliability of oxide TFTs.

Author Keywords

Polycrystalline Oxide Semiconductors (POS), Thin-Film Transistor (TFT), Indium Oxide (InO_x), Hydrogen-doping, High Mobility, Reliability.

1. Introduction

An amorphous oxide semiconductor (AOS) of In–Ga–Zn–O (a-IGZO)[1] has attracted attention for use in the active channel layer of thin-film transistors (TFT) due to its high field effect mobility (μ_{FE}>10 $cm^2V^{-1}s^{-1}$), large area uniformity, and extremely low off-current.[2] Although μ_{FE} of an a-IGZO TFT is over one order of magnitude higher than that of an amorphous Si TFT, further improvement of μ_{FE} of OS TFT is required to expand their range of applications. It is known that the Hall mobility of IGZO films can be improved by increasing the composition ratio of In_2O_3 because the conduction band minimum (E_{CBM}) of IGZO is composed of In 5s orbitals. Additionally, an addition of SnO_2 is also applied for IGZO (IGZTO) or IZO (ITZO) TFTs because the E_{CBM} tends to deepen with increasing contribution of 5*s* orbitals in In or Sn,[3] resulting in a reduction in the effective mass of electrons and an increase in μ_{FE} of the TFTs.[4] In contrast, increasing the amount of In or Sn ratios in AOS causes the generation of oxygen vacancies, showing the trade-off between the μ_{FE} and the threshold voltage (V_t) of AOS TFT. Most high-μ_{FE} AOS TFTs operate in the depletion mode with negative V_t values. Enhancement-mode operation is crucial for taking advantage of the extremely low off-current of oxide TFTs. Furthermore, the mobility-stability trade-off has been reported in high-μ_{FE} AOS TFT, especially under negative gate bias stress (NBS), because the carrier doping ability increases when the In or Sn content in AOS increases.[3] Although much effort has been made to achieve high-μ_{FE} enhancement-mode AOS TFT with good reliability, it is still a challenging topic.

In contrast, single-crystalline In_2O_3 exhibits a Hall mobility of more than 160 $cm^2V^{-1}s^{-1}$ with a carrier density of less than 10^{18} cm^{-3}, making polycrystalline InO_x a potential material for high-mobility TFT. A large-grain (~10 μm) polycrystalline IGO TFT was reported by Ebata et al.[5] in 2012. The IGO TFT operated in enhancement-mode with μ_{FE} and V_t values of 39.1 $cm^2V^{-1}s^{-1}$ and 1.4 V, respectively. The substituted Ga^{3+} ions at the In^{3+} sites in the bixbyite In_2O_3 crystal do not act as impurity scattering centers. In addition, Ga doping acts as a carrier suppressor in In_2O_3, which contributes to the operation of IGO TFT in the enhancement mode. Rabbi et al.[6] further increased the μ_{FE} of poly-IGO TFT to 78 $cm^2V^{-1}s^{-1}$; however, the TFT operated in the depletion mode with V_t of –1.07 V. Tsubuku et al.[7] reported the double-gate (DG) enhancement mode poly-IGO TFT with μ_{FE} of 28.3–41.4 $cm^2V^{-1}s^{-1}$; however, the DG poly-IGO TFT changed to depletion mode when μ_{FE} increased further to 55.7 $cm^2V^{-1}s^{-1}$. A trade-off between μ_{FE} and V_t has also been reported for polycrystalline OS TFT.

Our group reported hydrogen-doped poly-IGO and InO_x TFTs formed by solid-phase crystallization (SPC).[8-12] Hydrogen was introduced in the IGO and InO_x films during sputtering. The hydrogen in ambient sputtering reduced the nucleation density of the as-deposited amorphous films. The amorphous IGO:H and InO_x:H films were converted to a polycrystalline phase by low-temperature (250–350 °C) SPC. The grain size of the poly-IGO:H and InO_x:H films increased compared with that of those films without hydrogen doping because of the reduction of the nucleation density in the films.[11]

In this study, poly-InO_x:H TFTs with bottom-gate (BG) and self-aligned top-gate (SATG) structures were fabricated to investigate their electrical properties and reliability under bias and temperature stresses (BTS). The poly-InO_x:H TFTs operated in enhancement mode with μ_{FE} values of 32.0 for BG and 29.5 $cm^2V^{-1}s^{-1}$ for TG structures, respectively. The poly-InO_x:H TFTs exhibited excellent V_t stability under negative BTS (NBTS) conditions at 60 °C for 6000 s, irrespective of the TFT structure. No shift in V_t was observed in the NBTS test. These results demonstrate that polycrystalline oxides are strong candidates for opening a new route for achieving high-μ_{FE} and highly reliable TFTs.

2. Experiment and Results

2.1 Deposition of H-doped InO_x (InO_x:H) film

Indium oxide (InO_x) and hydrogen-doped InO_x (InO_x:H) films were deposited on a glass substrate via RF magnetron sputtering from an In_2O_3 target. Mixed gases of Ar/O_2 and $Ar/O_2/H_2$ were used to deposit InO_x and InO_x:H films, respectively. The O_2 gas ratio was set to 3% for both films, whereas the H_2 gas ratio was set to 5% for the InO_x:H film. The thickness of both the films was 30 nm. Both films were annealed at temperatures ranging from 100 °C to 400 °C. The crystallinity of the films was evaluated using X-ray diffraction (XRD) and

ISSN 0097-996X/25/5602-1009-$1.00 © 2025

electron backscattered diffraction (EBSD) analysis. The electrical properties were measured using Hall analysis.

2.2 Influence of H-doping on SPC poly-InO$_x$:H film

Figure 1 shows the XRD spectra of (a) InO$_x$ and (b) InO$_x$:H films before (as-deposited) and after annealing at 175, 200, and 250 °C in N_2 for 3 min. Both the as-deposited InO$_x$ and InO$_x$:H films were amorphous. No grains are observed in the EBSD analysis of the as-deposited films [Figs. 1(c) and 1(d)]. EBSD and XRD results revealed that the as-deposited InO$_x$ and InO$_x$:H films were amorphous.

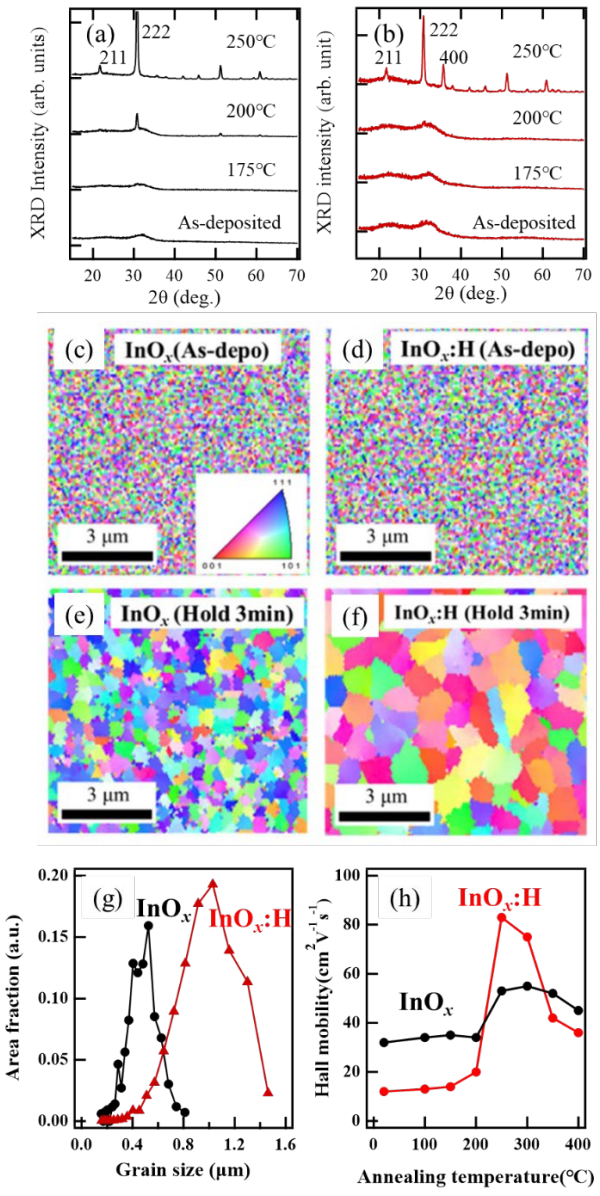

Figure 1 XRD spectra of (a) InO$_x$ and (b) InO$_x$:H films before and after annealing. EBSD images of (c, e) InO$_x$ and (d, f) InO$_x$:H films (c, d) before and (e, f) after SPC at 250 °C for 3 min. (g) Distributions of grain size in SPC InO$_x$ and InO$_x$:H films. (h) Hall mobility of InO$_x$ and InO$_x$:H films as a function of annealing temperature.[11)]

SPC was observed in both the films after annealing at 250 °C. The XRD results indicate that hydrogen doping in the InO$_x$ film did not influence the SPC temperature. However, the grain size of the film was markedly increased by hydrogen doping, as shown in Figs. 1(e) and 1(f). Figure 1(g) shows a comparison of the grain-size distributions of the InO$_x$ and InO$_x$:H films after SPC at 250 °C for 3 min. The average grain size of the film increased from 0.52 μm for the poly-InO$_x$ film to 1.03 μm for the poly-InO$_x$:H film. The hydrogen doping in the InO$_x$ film reduced the nucleation density from 4.1 to 1.1 μm^{-2}, resulting in an increase in grain size of the poly-InO$_x$:H film.[11)] Figure 1(h) shows a comparison of Hall mobility between the InO$_x$ and InO$_x$:H films as a function of annealing temperature. Annealing was performed for 3 min under an ambient N_2 atmosphere. After SPC at 250 °C, the Hall mobility increased from 47 $cm^2V^{-1}s^{-1}$ for the poly-InO$_x$ film to 83 $cm^2V^{-1}s^{-1}$ for the poly-InO$_x$ film, owing to an increase in grain size. The results indicate that hydrogen doping in the InO$_x$ film plays an important role in increasing the grain size and improving the Hall mobility. Notably, the InO$_x$:H film was completely converted into a polycrystalline phase after SPC at 250 °C for 3 min without an amorphous region, as shown in Fig. 1(f). The low-temperature (250 °C) and fast (3 min) SPC processes of the InO$_x$:H film provide a great advantage for the mass production of poly-InO$_x$:H TFT.

Both BG and SATG poly-InO$_x$:H TFTs are presented in the next section.

2.3 Electrical properties and reliability of poly-InO$_x$:H TFT

2.3.1 Fabrication process steps for poly-InO$_x$:H TFTs with BG and SATG structures

Figure 2 shows the fabrication process steps for (a) BG and (c) SATG poly-InO$_x$:H TFTs. The microscopic top views of the (b) BG and (d) SATG poly-InO$_x$:H TFTs are shown in Fig. 2.

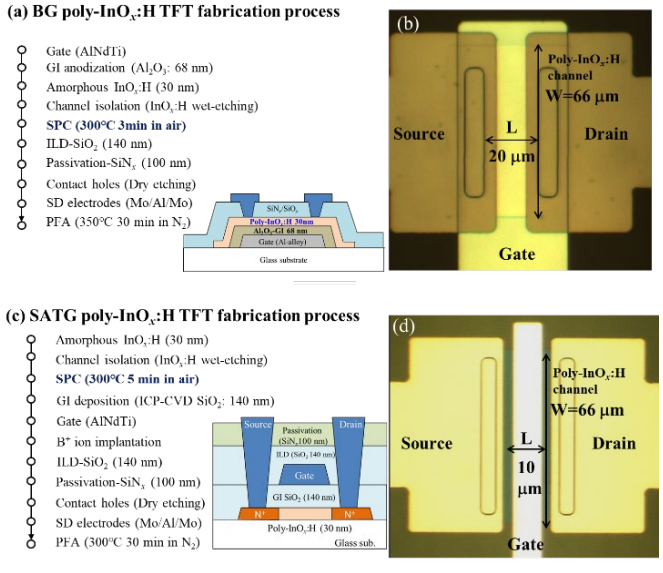

Figure 2. Fabrication process steps for poly-InO$_x$:H TFTs with (a) BG and (c) SATG structures. Microscopic top-view of (b) BG and (d) SATG poly-InO$_x$:H TFT.

The 30 nm-thick poly-InO_x:H film, which was formed by SPC at 300 °C in air, was used as a channel for both TFT.

For the BG poly-InO_x:H TFT, a 68 nm-thick high-k Al_2O_3 gate insulator (GI) was formed by anodizing the gate electrode (Al alloy) surface. The detailed fabrication process of the BG poly-InO_x:H TFT is published in Ref 12.

For the SATG poly-InO_x:H TFT, a 140 nm-thick hydrogen-free (H-free) SiO_2 film deposited by inductively coupled plasma chemical vapor deposition (ICP-CVD) was used as the GI. After the Al-alloy gate electrodes were fabricated, boron ions were implanted through the GI to form source and drain (S/D) regions in a self-aligned manner. Then 140 nm-thick H-free SiO_2 and 100 nm-thick H-free SiN_x films were sequentially deposited by ICP-CVD for interlayer dielectric (ILD) and passivation (PVL), respectively. Note that the hydrogen concentration in the GI, ILD, and PVL was estimated to be less than 3×10^{19} cm^{-3}, which is more than two orders of magnitude lower than that in conventional PECVD SiO_2 and SiN_x films. After the contact holes were opened, the S/D electrodes were formed.

2.3.2 Electrical properties of BG and SATG poly-InO_x:H TFT

Figure 3 shows the transfer characteristics of (a) BG and (b) SATG poly-InO_x:H TFTs after post-fabrication annealing (PFA). The μ_{FE} was extracted from the transconductance in the linear region at a drain voltage (V_{DS}) of 0.1 V. V_t was defined by a gate voltage (V_{GS}) at the I_{DS} of (W/L)×1 nA. Both TFTs exhibited good switching properties and operated in enhancement mode with V_t values of 0.58 V for the BG and 0.17 V for the SATG TFTs. The μ_{FE} value of the BG (32.0 $cm^2V^{-1}s^{-1}$) is slightly larger than that of the SATG (29.5 $cm^2V^{-1}s^{-1}$) TFT. This is due to the fact that the gate capacitance of the GI-Al_2O_3 in the BG TFT is greater than that of the GI-SiO_2 in the SATG TFTs, resulting in an increase of a sheet carrier concentration in the poly-InO_x:H channel under the accumulation condition. The high-k GI-Al_2O_3 in the BG TFT also contributed to improving the sub-threshold swing (*S.S.*) value. A summary of the electrical properties of both the BG and SATG poly-InOx:H TFTs is presented in Table 1.

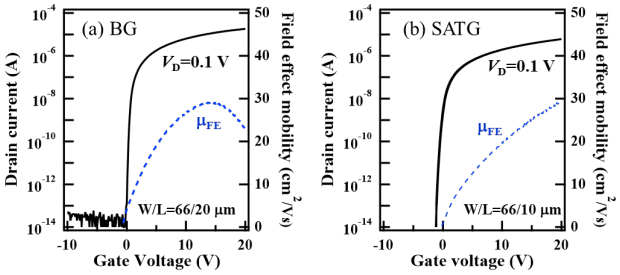

Figure 3. Transfer characteristics of (a) BG and (b) SATG poly-InO_x:H TFTs.

Table 1. Summary of the electrical properties of poly-InO_x:H TFTs extracted from BG and SATG structures.

TFT structure	μ_{FE} ($cm^2V^{-1}s^{-1}$)	V_t (V)	S.S. (V/dec.)
BG	32.0	0.58	0.13
SATG	29.5	0.17	0.30

2.3.3 Reliability of BG and SATG poly-InO_x:H TFT

The reliability of poly-InO_x:H TFT is an important consideration in practical applications. The evolution of the transfer characteristics was measured under negative and positive gate biases and temperature stresses (NBTS and PBTS, respectively) for BG and TGSA structures.

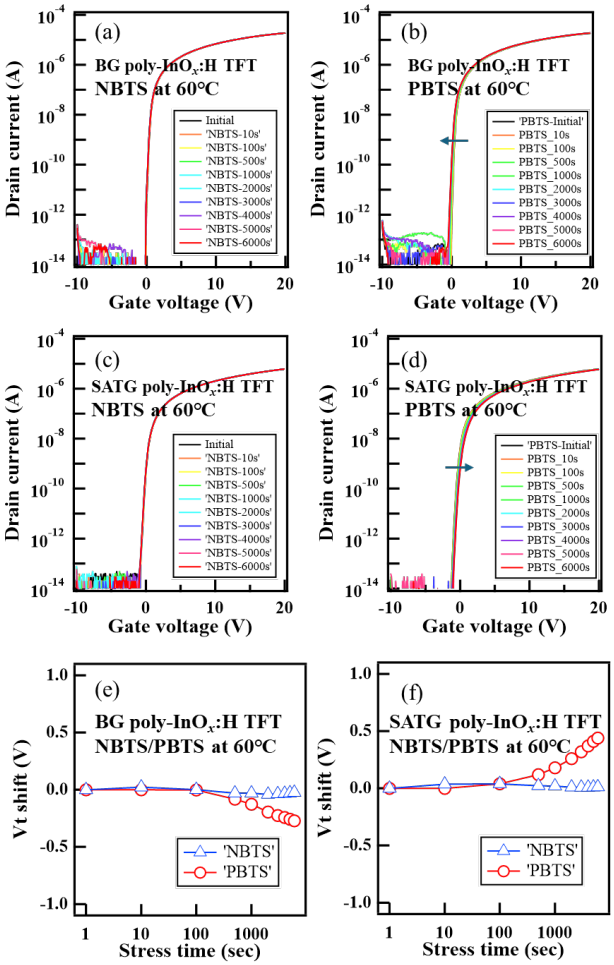

Figure 4. Evolution of transfer characteristics of (a, b) BG and (c, d) SATG poly-InO_x:H TFTs under (a, c) NBTS and (b, d) PBTS. Stress-time dependence of V_{th} shift under NBTS and PBTS obtained from (e) BG and (f) SATG poly-InO_x TFTs.

From the NBTS tests, as shown in Figs. 4(a) and 4(c), both BG and SATG poly-InO_x:H TFTs exhibited excellent reliability. No shift in V_t was observed under NBTS at 60 °C after a stress time of 6,000 s. Since the poly-InO_x:H channel was fully depleted by the NBTS, the V_t instability mainly originated from the Fermi level shift in the channel owing to the activation of shallow donor defects. It is worth noting that hydrogen in the poly-InO_x:H channel was not activated by NBTS although the poly-InO_x:H film contained 8.6 atom% hydrogen after SPC.[10)]

The V_t instability of PBTS is mainly caused by electron trapping at the GI/poly-InO_x:H channel interface or in the GI, because electrons are accumulated by PBTS at the GI/channel interface. From the BG poly-InO_x:H TFT with GI-Al_2O_3, as

shown in Fig. 4(b), PBTS exhibited a small negative V_t shift of -0.27 V after 6,000 s. One of the possible causes of the negative V_t shift is the presence of mobile positive ions in the GI of Al_2O_3, because Al_2O_3 is formed by anodization in a wet solution. On the other hand, from the SATG poly-InO_x:H TFT with GI-SiO_2 as shown in Fig. 4(d), PBTS observed a positive V_t shift of 0.44 V after 6,000 s due to electron trapping in the GI/poly-InO_x:H channel or in the GI. The reliability of PBTS can be improved in future research by optimizing the GI/poly-InO_x:H interface or the GI. Figure 4 also shows the stress-time dependence of the V_t shift under NBTS and PBTS obtained from (e) BG and (f) SATG poly-InO_x:H TFTs.

3. Conclusion

We demonstrate poly-InO_x:H TFTs with BG and SATG structures. The poly-InOx:H channel was formed by low-temperature SPC using a hydrogen-doped amorphous InO_x:H film. Hydrogen doping of the InO_x film reduced the nucleation density in the film, resulting in an increase in the grain size of the poly-InO_x:H film after SPC. Furthermore, the amorphous InO_x:H film was completely converted into a poly-InOx:H film after SPC at 250 °C for 3 min. The low-temperature (250 °C) and fast (3 min) SPC processes of the InO_x:H film provide a great advantage for the mass production of poly-InO_x:H TFT. Both the BG and SATG poly-InO_x:H TFTs operated in enhancement mode with field-effect mobilities of 32.0 $cm^2V^{-1}s^{-1}$ for BG and 29.5 $cm^2V^{-1}s^{-1}$for SATG. The poly-InO_x:H TFTs exhibited excellent stability under a negative gate bias and temperature stress, irrespective of the TFT structure. These results demonstrate that poly-oxide is a strong candidate for opening a new route to improve the mobility and reliability of oxide TFTs.

4. Acknowledgements

This research was supported in part by the Japan Society for the Promotion of Science (JSPS) KAKENHI (grant number 22K04200). The EBSD analysis was supported by the Advanced Research Infrastructure for Materials and Nanotechnology (ARIM), Ministry of Education, Culture, Sports, Science, and Technology (MEXT), Japan (Proposition No. JPMXP1223HK0102). The authors would like to thank Tokyo Electron Technology Solutions Ltd., Nissin Ion Equipment Co., Ltd., Mitsui Kinzoku Co., Ltd., and Idemitsu Kosan Co., Ltd. for their support in the TFT fabrication.

5. References

1. Nomura K, Ohta H, Takagi A, Kamiya T, Hirano M, Hosono H. Room-temperature fabrication of transparent flexible thin-film transistors using amorphous oxide semiconductors. Nature. 2004 Nov 25; 432(7016):488-92. https://doi.org/10.1038/nature03090
2. Kato, K., Shionoiri, Y., Sekine, Y., Furutani, K., Hatano, T., Aoki, T., Sasaki, M., Tomatsu, H., Koyama, J., Yamazaki, S. Evaluation of off-state current characteristics of transistor using oxide semiconductor material, indium-gallium-Zinc oxide Jpn. J. Appl. Phys., 51 (2012) 021201 http://dx.doi.org/10.1143/JJAP.51.021201
3. Shiah, Y. S., Sim, K., Shi, Y., *et al.* Mobility–stability trade-off in oxide thin-film transistors. *Nat Electron* **4**, 800–807 (2021). https://doi.org/10.1038/s41928-021-00671-0
4. Yang, H., Zhang, Y., Matsuo, Y., Magari, Y., and Ohta, H., Thermopower Modulation Analyses of High-Mobility Transparent Amorphous Oxide Semiconductor Thin-Film Transistors. ACS Applied Electronic Materials 2022 4 (10), 5081-5086 https://doi.org/10.1021/acsaelm.2c01210
5. Ebata, K., Tomai, S., Tsuruma, Y., Iitsuka, T., Matsuzaki, S., and Yano, K., High-Mobility Thin-Film Transistors with Polycrystalline In–Ga–O Channel Fabricated by DC Magnetron Sputtering. *Appl. Phys. Express* **5** 011102 (2012) http://dx.doi.org/10.1143/APEX.5.011102
6. Rabbi, MH., Lee, S., Sasaki, D., Kawashima, E., Tsuruma, Y., Jang, J., Polycrystalline InGaO Thin-Film Transistors with Coplanar Structure Exhibiting Average Mobility of ≈78 cm^2 V^{-1} s^{-1} and Excellent Stability for Replacing Current Poly-Si Thin-Film Transistors for Organic Light-Emitting Diode Displays. *Small Methods* 2022, 6, 2200668. https://doi.org/10.1002/smtd.202200668
7. Tsubuku, M., Watakabe, H., Sasaki, T., Tamaru, T., Onodera, R., Mochizuki, M., Kimura, H., Kawashima, E., Sasaki, D. and Tsuruma, Y. (2023), 8-1: *Invited Paper:* High Mobility Poly-Crystalline Oxide TFT Achieving Mobility over 50 cm^2/Vs and High Level of Uniformity on the Large Size Substrates. SID Symposium Digest of Technical Papers, 54: 78-81. https://doi.org/10.1002/sdtp.16492
8. Furuta, M., Shimpo, K., Kataoka, T., Tanaka, D., Matsumura, T., Magari, Y., Velichko, R., Sasaki, D., Kawashima, E. and Tsuruma, Y. (2021), 7-4: High Mobility Hydrogenated Polycrystalline In-Ga-O (IGO:H) Thin-Film Transistors formed by Solid Phase Crystallization. SID Symposium Digest of Technical Papers, 52: 69-72. https://doi.org/10.1002/sdtp.14612
9. Magari, Y., Kataoka, T., Yeh, W. Furuta, M. High-mobility hydrogenated polycrystalline In_2O_3 (In_2O_3:H) thin-film transistors. *Nat Commun* **13**, 1078 (2022). https://doi.org/10.1038/s41467-022-28480-9
10. Kataoka, T., Magari, Y., Makino, H., Furuta, M. Nondegenerate Polycrystalline Hydrogen-Doped Indium Oxide (InOx:H) Thin Films Formed by Low-Temperature Solid-Phase Crystallization for Thin Film Transistors. *Materials* **2022**, *15*(1),187 https://doi.org/10.3390/ma15010187
11. Wang, X., Magari, Y., Furuta, M. *et al* 2024 Nucleation and grain growth in low-temperature rapid solid-phase crystallization of hydrogen-doped indium oxide. *Jpn. J. Appl. Phys.* **63** 03SP38 https://doi.org/10.35848/1347-4065/ad21ba
12. Okamoto, N., Wang, X., Morita, K., Kato, Y., Alom, M M., Magari, Y., Uniformity and Reliability of Enhancement-Mode Polycrystalline Indium Oxide Thin Film Transistors Formed by Solid-Phase Crystallization. *IEEE Electron Device Letters*, vol. 45, no. 12, pp. 2403-2406, Dec. 2024, https://doi.org/10.1109/LED.2024.3480991